Elastic properties of model random three-dimensional open-cell solids

by

A. P. Roberts
Centre for Microscopy and Microanalysis
University of Queensland
St. Lucia, Queensland 4072 AUSTRALIA

and

E. J. Garboczi
Building and Fire Research Laboratory
National lnstitute of Standards and Technology
Gaithersburg, MD 20899 USA

Reprinted **from** the Journal of the Mechanics and Physics of Solids, Vol. 50, No. I, **33-55, 2002.**

National Institute of Standards and Technology
Technology Administration, **U.S.** Deportment of Commerce

PERGAMON

Journal of the Mechanics and Physics of Solids
50 (2002) 33–55

JOURNAL OF THE
MECHANICS AND
PHYSICS OF SOLIDS

www.elsevier.com/locate/jmps

Elastic properties of model random three-dimensional open-cell solids

A.P. Roberts[a,b,*], E.J. Garboczi[a]

[a] *Building Materials Division, National Institute of Standards and Technology, Gaithersburg, MD 20899, USA*

[b] *Centre for Microscopy and Microanalysis, University of Queensland, St. Lucia, Queensland 4072, Australia*

Received 7 November 2000; received in revised form 20 March 2001; accepted 7 April 2001

Abstract

Most cellular solids are random materials, while practically all theoretical structure–property relations are for periodic models. To generate theoretical results for random models the finite element method (FEM) was used to study the elastic properties of open-cell solids. We have computed the density (ρ) and microstructure dependence of the Young's modulus (E) and Poisson's ratio (ν) for four different isotropic random models. The models were based on Voronoi tessellations, level-cut Gaussian random fields, and nearest neighbour node-bond rules. These models were chosen to broadly represent the structure of foamed solids and other (non-foamed) cellular materials. At low densities, the Young's modulus can be described by the relation $E \propto \rho^n$. The exponent n and constant of proportionality depend on microstructure. We find $1.3 < n < 3$, indicating a more complex dependence than indicated by periodic cell theories, which predict $n = 1$ or 2. The observed variance in the exponent was found to be consistent with experimental data. At low densities we found that $\nu \approx 0.25$ for three of the four models studied. In contrast, the Voronoi tessellation, which is a common model of foams, became approximately incompressible ($\nu \approx 0.5$). This behaviour is not commonly observed experimentally. Our studies showed the result was robust to polydispersity and that a relatively large number (15%) of the bonds must be broken to significantly reduce the low-density Poission's ratio to $\nu \approx 0.33$.

Keywords: Structure-property relationships; A. Microstructures; B. Foam material; C. Finite elements; C. Probability and statistics

* Corresponding author. Permanent address: Centre for Microscopy and Microanalysis, University of Queensland, St. Lucia, Queensland 4072, Australia. Tel.: +61-7-3365-4947; fax: +61-7-3365-4422.

E-mail address: anthony.roberts@mailbox.uq.edu.au (A.P. Roberts).

0022-5096/01/$ - see front matter
PII: S0022-5096(01)00056-4

I. Introduction

Manufactured cellular materials have been developed for a range of applications (Gibson and Ashby, 1988) (e.g. insulation, light-weight reinforcement. and filtration), and their natural counterparts (e.g. bone. sponge and wood) have a cellular structure that optimises performance in a particular setting. The useful properties of cellular solids depend on the material from which they are made. their relative density, and their internal geometrical structure. It is important to link the physical properties of cellular solids to their density and complex microstructure. in order to understand how such properties can be optimised for a given application. Many studies have focused on how local cell features, such as strut shape, affect the properties of periodic arrays of cells. Some theoretical results for such models are generalisable to real materials, but some are not. Equally important is the effect of disorder (e.g., isotropy), and the interaction between cells on a rnesoscopic scale, as most real cellular solids are not periodic. In this paper we study model isotropic cellular solids at scales (≈ 100 cells) where these effects can be probed. Since no exact results exist for random porous materials, new large-scale computational methods for analysing random microstructure provide the only means of understanding their complex structure–property relationships. This type of study has not been previously undertaken for three-dimensional models, and is expected to yield new results. Our primary aim is to provide simple and accurate structure–property relations for realistic models of cellular solids. The results also allow us to test the validity of using simple (e.g. periodic) models to predict the properties of random porous materials.

At low densities. experimental results indicate that Young's modulus (E) of cellular solids is related to their density (ρ) through the relation (Gibson and Ashby, 1988):

$$\frac{E}{E_s} = C\left(\frac{\rho}{\rho_s}\right)^n = Cp^n \tag{1}$$

where E_s and ρ_s are the Young's modulus and density of the solid skeleton and $p = \rho/\rho_s$ is the reduced density. The constants C and n depend on the microstructure of the solid material. Similar relations hold for the bulk and shear moduli, with possibly different values of C and n. The value of n generally lies in the range $1 \leqslant n < 4$, giving a wide range of properties at a given density. Experimental evidence suggests that $n = 2$ for open cells. The Poisson's ratio has been thought to be independent of density (Gibson and Ashby. 1988).

The complex dependence of C and n on microstructure is not well understood. and this remains a crucial problem in the ability to predict and optimise the elastic propenies of cellular solids. At the local or cellular scale. important variables include the cell character (e.g. open or closed), the geometrical arrangement of the cell elements (e.g. angle of intersection), and the shape of the cell struts or walls (e.g. curvature. and cross-sectional shape and uniformity). At a larger scale. the geometrical arrangement of the cells is also crucial. The values of both C and n will depend on whether the material is periodic or disordered.

Most theoretical attention has been focused on simple three-dimensional cell structures with straight struts (or walls) arranged in periodic arrays at low densities. In

this limit, explicit solution of the equations of elasticity can be avoided by using thin beam or plate theories. These results have elucidated some of the basic mechanisms of deformation. and their influence on the overall properties.

If a periodic open-cell solid has 'straight-through' struts that traverse the extent of the sample. deformation occurs along the strut axis, and the moduli varies in direct proportion to the density (Cent and Thomas, 1959: Ko, 1965; Christensen. 1986) ($n=1$). If the struts are finite. bending is activated at their intersection points and the Young's modulus can be shown tu vary quadratically with the density (Ko, 1965; Gibson and Ashby. 1982: Warren and Kraynik. 1997) ($n=2$) in agreement with experiment. In addition. the importance of strut twisting has also been considered (Warren et al., 1997).

The 'tetrakaidecshedral' foam model, in particular. has been the subject of many recent studies (Zhu et al., 1997a; Warren and Kraynik. 1997: Grenestedt, 1999: Christensen, 2000). The cells of the model uniformly partition space, and are defined by truncating the comers of a cube giving eight hexagonal and six square faces. The foam has a relatively low anisotropy (Zhu et al.. 1997a) (the Young's modulus varies by less than 10% with direction of loading), and is thought to be a good model of isotropic foams. However, the model exhibits unusual behaviour that has not been confirmed in real materials. Specifically, the Young's modulus varies quadratically with density but the bulk modulus only varies linearly with density (Zhu et al., 1997a; Warren and Kraynik, 1997). In the low-density limits this corresponds to a Poisson's ratio of $\nu \approx 0.5$ indicating nearly incompressible behaviour. In contrast, typical foams have $0.1 < \nu < 0.4$ (Lakes, 1987).

There have been several attempts to incorporate isotropy in simple models of cellular structures. Christensen (1986) treated the case of straight-through struts. which does not reproduce the quadratic density dependence of either the bulk or Young's modulus, while Warren and Kraynik (1988) examined the case of a rotationally averaged tetrahedral joint. The model predicts the same unusual linear dependence of the bulk modulus on density as the tetrakaidecahedral model. As barren and Kraynik (1997) note, regular tetrahedra do not pack to fill space. and so the model cannot represent a real foam.

From the foregoing discussion it is clear that more complex random models are necessary to improve predictions for cellular solids. since periodic models do not capture all the phenomena observable in real cellular solids. There are two main problems in studying random models. First. a sufficiently accurate model of the microstructure must be developed. Second. the properties of the model must be accurately evaluated. We emphasise that there are no exact analytical calculations available for general random materials. so that numerical methods become necessary.

Large-scale computational methods (Garboczi and Day, 1995; Poutet et al., 1996) and sufficient computational power now exist for measuring the properties of complex digital microstructures with a reasonable degree of complexity. One route for property prediction is to directly image the porous structure. and then use a numerical method to predicts its moduli (Nieh et al., 1998). This method can work well for a particular microstructure. However, it is also important to study how changes in microstructure affect properties (e.g., to guide optimisation). Statistical models. which allow variation of the density and structure. are ideally suited for this purpose.

There has been recent progress in this direction. Disorder and imperfections have been shown to play a significant role in degrading the stiffness and strength of two-dimensional structures (Silva et al., 1997; Chen et al., 1999). It is important to extend these studies to three dimensions in order to make quantitative statements about isotropic materials. Finite element methods have been used to study the properties of three-dimensional random open-cell Voronoi tessellations (Van der Burg et al., 1997). The similarities between the mathematical definition of the Voronoi tessellation and the physics of foam formation make the model a natural choice for cellular solids. A key question is whether the model can account for the properties of real cellular materials. As discussed above, the tetrakaidecahedral model, which is an example of the tessellation of a regular lattice, actually exhibits approximately incompressible behaviour in the low-density limit. It is interesting to see if this behaviour is due to the inherent nature of the tessellation. Two-dimensional studies of random tessellations do show near incompressibility (Silva et al., 1997), and it is therefore interesting to study the three-dimensional case. Since foaming is only one route to generating cellular solids (Gibson and Ashby, 1988), it is useful to investigate different types of cellular structures via alternate statistical models.

In this paper we use a finite element method (FEM) (Garboczi and Day, 1995) to estimate the elastic properties of four model cellular solids over a range of densities. The models are generated using tessellation methods (Stoyan et al., 1995), level-cut random field models (Berk, 1987), or by simply linking random nodes in space with struts. The models each have distinct microstructures, and are chosen to be broadly representative of the morphologies observed in real materials. The Young's moduli of the models can be described in terms of simple two parameter relations [e.g. Eq. (1) in the low-density limit]. The results demonstrate the effect of microstructure, isotropic disorder. and finite density on the properties of cellular solids, including both Young's modulus and Poisson's ratio. The results can be used to predict the properties of cellular solids if their structure is similar to one of the models, or be used to accurately interpret experimental data.

2. Theoretical and semi-empirical models

We first review a selection of results that are available for periodic cellular solids. The results illustrate the basic mechanisms of deformation, and provide benchmark tests for the FEM. These results, gathered from the literature, also provide useful comparisons with the FEM results for random models discussed in subsequent sections.

First consider a simple cubic array of uniformly spaced intersecting aligned struts. From elementary considerations, the Young's modulus is $E/E_s \approx \frac{1}{3}(\rho/\rho_s)$ for uniaxial compression along a strut axis. The linear dependence of modulus on density is typical of model foams that contain 'straight-through' struts that traverse the extent of the sample; longitudinal compression or tension being the only mode of deformation (Christensen, 1986; Warren and Kraynik, 1988; Zhu et al., 1997a).

Since most foams do not contain straight-through struts, beam bending comes into play (Ko, 1965; Gibson and Ashby. 1982; Warren and Kraynik, 1988; Zhu et al.,

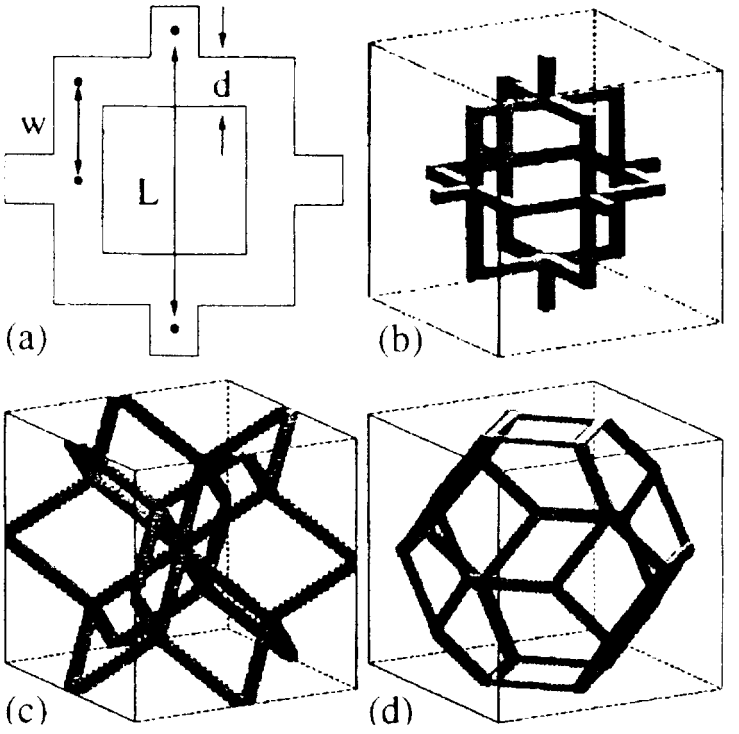

Fig. 1. Periodic models of open-cell solids. (a) The parameters used to define a simple model. (b) A 3-D version of the simple model. (c) An open-cell foam considered by Ko (1965). (d) A unit cell of the tetrakaidecahedral model.

1997a). This is most easily seen in the unit cell of the simple open-cell model shown in Fig. 1(b). The cell is a modification of the model shown in Fig. 5.6 of Gibson and Ashby's (1988) book. since the original model could not be periodically extended. The solid fraction is

$$\frac{\rho}{\rho_s} = \frac{3d^2L + 18wd^2 - 6d^3}{(L+d)^3} \approx \frac{d^2}{L^2}\left(3 + 18\,\frac{w}{L}\right), \tag{2}$$

where the approximation is for thin beams $d \ll w, L$, and the length scale parameters are shown in Fig. 1(a). Now consider the deformation of the cell if it is compressed along the x-axis (100 axis) by a force f. The Young's modulus is $E = (f/L^2)/(\delta L/L)$ where δL is the total deformation. From thin beam theory (Landau and Lifshitz, 1959), the deformation of a thin beam of half-length w with clamped ends due to an applied force f is $\delta L = f w^3/24 E_s I_m$. Here I_m is the principal moment of inertia. with $I_m = d^4/12$ for a square beam of width d. The deformation is halved because two beams intersect at the point of application. but as this occurs twice in the unit cell the total deformation is the same as that for a single beam. Thus in the thin-beam limit we have.

$$\frac{E_{100}}{E_s} = \frac{2d^4}{L^3}\left(3 + 18\,\frac{w}{L}\right) \tag{3}$$

The quadratic dependence of the modulus on density is typical of foams where beam bending is the principle mechanism of detormation. Ko (1965) demonstrated this behaviour for the model shown in **Fig.** 1(a) loaded in the (111) direction. Note that

the calculation leading to **Eq.** (3) is illustrative only. In reality, the beam ends are not clamped, so the pre-factor is only an approximation.

Zhu et al. (1997a) and Warren and Kraynik (1997) derived analytic results for the open-cell tetrakaidecahedral model (Fig. 1(d)) packed in a body-centred cubic array. The results provide a useful check of the FEM (see Section 3). and demonstrate incompressible behaviour ($\nu \to 0.5$) at low densities. The results of Zhu et al. for the Young's modulus and Poisson's ratio for strain parallel to the $\langle 1\,0\,0\rangle$ axis are,

$$\frac{E_{100}}{E_s} = \frac{2}{3} C_Z \left(\frac{\rho}{\rho_s}\right)^2 \left(1 + C_Z \frac{\rho}{\rho_s}\right)^{-1}, \qquad \nu_{12} = \frac{1}{2}\left(\frac{1 - C_Z(\rho/\rho_s)}{1 + C_Z(\rho/\rho_s)}\right), \tag{4}$$

where $C_Z = 8\sqrt{2}I/A^2$ depends on the cross-sectional area A and the second moment of the area I. For equilateral triangles $C_Z = 1.09$ (Zhu et al., 1997a), and for cylindrical beams $C_Z = 0.900$. Note that the Poisson's ratio depends on orientation. The notation ν_{12} corresponds to expansion measured in the $\langle 0\,1\,0\rangle$ or $\langle 0\,0\,1\rangle$ directions. **As** mentioned above, the foam is relatively stiff under uniform compression, with the bulk modulus given by $K/E_s = \frac{1}{9}\rho/\rho_s$.

We now review semi-empirical and analytic results for random foams. The most commonly used result for open-cell foams is (Gibson and Ashby, 1988)

$$\frac{E}{E_s} \approx C\left(\frac{\rho}{\rho_s}\right)^2, \qquad \nu \approx \frac{1}{3}, \tag{5}$$

where the pre-factor $C \approx 1$ and Poisson's ratio have been empirically determined. This semi-empirical formula broadly describes data obtained for many different types of foams.

There have also been several methods proposed to derive analytic predictions for isotropic foams. **A** typical result, which performs an isotropic average of randomly placed long thin (i.e. straight-through) struts. has been derived by Christensen (1986).

$$\frac{E}{E_s} = \frac{1}{6}\left(\frac{\rho}{\rho_s}\right), \qquad \nu = \frac{1}{4}. \tag{6}$$

Christensen notes that the results are equivalent to those of Gent and Thomas (1959). In the low-density limit. the same results have been derived for a rotationally averaged simple cubic structure (Warren and Kraynik. 1988). The absence of bending in these models is indicated by the linear dependence of the Young's modulus on density.

Warren and Kraynik (1988) have derived analytic results for the properties of a foam comprised **of** isotropically oriented tetrahedrally arranged struts. The geometry can be visualised as a node located at the centre **of** a tetrahedron with equilateral faces, the four struts (separated by an angle of 109.5°) connecting the central node to the vertices. There are eight nodes of this type adjacent to the central node in Fig. 1(c). The results are

$$\frac{E}{E_s} = \frac{C_W p^2(11 + 4C_W p)}{10 + 31C_W p + 4C_W^2 p^2}, \qquad \nu = \frac{1}{2}\frac{(1 - C_W p)(10 - 8C_W p)}{10 - 31C_W p + 4C_W^2 p^2} \tag{7}$$

where $p = \rho/\rho_s$ and $C_W = 18I/\sqrt{3}A^2$. For struts of equilateral triangular cross-section $C_W = 1$, while for a circular cross-section $C_W \approx 0.827$ **As** expected from the definition

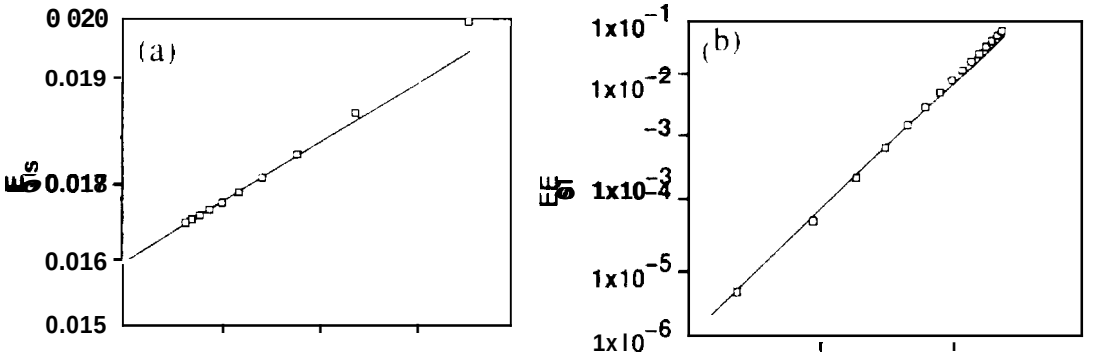

of the model, beam bending is the primary mode of deformation for uniaxial compression. However, Eqs. (7) imply $K'E_s = \frac{1}{9}p$ indicating that bending is not activated under pure compression. Like the tetrakaidecahedral model, the Poisson's ratio of the model therefore tends to 0.5 at low densities.

3. Elastic properties of model cellular solids

The finite element method uses a variational fonnulation of the linear elastic equations. and finds the solution by minimising the elastic energy via a fast conjugate gradient method. The digital image is assumed to have complete periodic boundary conditions. Details of the theory and copies of the actual programs used are reported in the papers of Garboczi and Day (1995) and Garboczi (1998).

Given a digital microstructure. the FEM provides a numerical solution of the elasticity equations. The accuracy is only limited by the finite number of pixels which can be used (around 10^6 in this study). We consider continuum models with a fixed length scale, such as cell size. and measure the properties of a $T \times T \times T$ μm region. divided into M^3 cubic pixels. Here T is much greater than the cell size. If the foam were regular and periodic. just one unit cell would be sufficient. In this section we discuss the sources of error and how they can be minimised.

Discretisation errors occur in the FEM when there are insufficient pixels in a solid region to correctly model continuum elasticity. To check the effect of resolution for the FEM we measured the Young's modulus of the simple cell model shown in Fig. 1(b) (with $L = 6$. $w = 2$ and $d = 1$ μm) at finer and finer resolutions $M = 7, 14, \ldots, 77$. Here. and in subsequent calculations. we use $E_s = 1$ GPa and a solid Poisson's ratio of $\nu_s = 0.2$. The results are shown in Fig. 2(a). An empirical tit of the foam $E_{FEM} \approx E_{true} - aM^{-1}$ is used to determine the 'exact' modulus: the linear nature of the graph (Fig. 2(a)) for $M > 21$ confirms the ansatz. The error is less than 10% for $M \geqslant 28$. which corresponds to a strut thickness of four pixels. As the square beams have

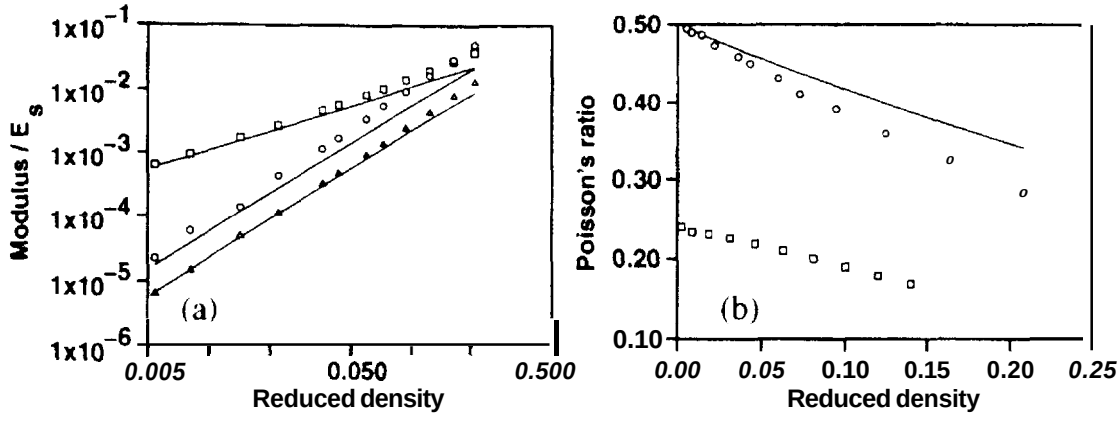

Fig. 3. The properties of tetrakaidecahedral cell model shown in Fig. 1(d) as a function of density. (a) The Young's (○), bulk (□) and shear (Δ) modulus. The lines correspond to Eq. (4) with $C_Z = -0.9$. (b) The Poisson ratio ν_{12} (○) compared with theory (line) [Eq. (4). $C_Z = 0.9$]. The results (□) for the simple cell model shown in Fig. 1(b) are also plotted.

stress concentrations at the comers, we expect the code will perform better for model foams with rounded edges. The extrapolated numerical value $E_{exact}/E_s = 0.16$ is 20% higher than the theoretical value $E_{100}/E_s = 0.13$ [Eq. (3)], the difference being attributed to the finite density of the model ($\rho/\rho_s = 0.14$) and the assumption of clamped ends.

To check the density dependence of Eq. (3) we measured the Young's modulus and Poisson's ratio of the simple cell model. We used the parameters $L = 60$, $n = 20\,\mu m$ and varied d over the range 1–15 μm at a resolution of 1 μm/pixel (giving a density range of $\rho/\rho_s = 0.0024$–0.24). The results for E_{100} are shown in Fig. 2(b) and confirm that Eq. (3) with $C = \frac{2}{3}$ is a reasonable approximation.

We also measured the properties of the open-cell tetrakaidecahedral model (Fig. 1(d)) with cylindrical struts. We employed a unit-cell size of $M = 80$ pixels with side length $T = 80\,\mu m$ and vaned the cylinder radius in the range $r = 1$–$8\,\mu m$. The results, shown in Fig. 3(a), approximately agree with the theoretical formulae [Eq. (4) with $C_Z = 0.9$] in the low density limit. In Fig. 3(b) we show ν_{12} as a function of density, as well as ν_{12} for the simple cell model (Fig. 1(b)), which does not exhibit incompressible behaviour.

For random foams, we also need to consider finite size effects. If there are too few cells in the computational cube. the estimates will not correspond to the properties of a macroscopic system (which may have many thousands of cells). Preliminary studies indicated that about 100 cells are necessary (roughly five cells in each direction) to keep the finite size errors of the same order as the discretisation errors. Finally, one has to determine the number of samples N_s that need to be studied to ensure that the statistical variation of individual samples does not bias the results. For the sample size considered, we found five samples were sufficient. The resulting statistical errors were generally less than 10%, but at the lowest densities we measured, could increase to 20%.

In this study we restrict attention to the case where the Poisson's ratio of the solid material is $\nu_s = 0.2$. For general porous three-dimensional materials we have

recently shown (Roberts and Garboczi, 2001) that the Young's modulus is practically independent (to within 3%) of ν_s. Moreover, at low densities, the Poisson ratio of the porous material also becomes independent of ν_s.

3.1. *Voronoi tessellations*

The most common models of cellular solids are generated by Voronoi tessellation of distributions of 'seed points' in space. Around each seed there is a region of space that is closer to that seed than any other. This region defines the cell of a Voronoi (or Dinchlet) tessellation (Stoyan et al., 1995). Placing a solid wall at each face of these cells results in a closed-cell Voronoi tessellation. An open-cell Voronoi tessellation results if only the edges where two cell walls intersect are defined as solid. For several different random (e.g. Poisson) distributions of seed-points, the average number of faces per cell falls in the range 13.7–15.5 (Oger et al., 1996).

The Voronoi tessellation can also be obtained (Stoyan et al., 1995) by allowing spherical bubbles to grow with uniform velocity from each of the seed points. Where two bubbles touch, growth is halted at the contact point, but allowed to continue elsewhere. In this respect the tessellation is similar to the actual process of **liquid** foam formation (Van der Burg et al., 1997). Of course, physical constraints such as minimisation of surface energy will also play an important role. Depending on the properties of the liquid and the processing conditions, the resultant solid foam will be comprised of open and/or closed cells.

The amount of order in the Voronoi tessellation depends on the order in the seed points. If regular arrays are such, ordered anisotropic foams will result. Indeed the open-cell models used by Warren and Kraynik (1997), Zhu et al. (1997a) and Ko (1965) turn out to be equivalent to Voronoi tessellations of the body-centered cubic (BCC) (Fig. 1(d)), face-centered cubic (Fig. 1(c)), and hexagonal close-packed lattices. If a purely random (Poisson) distribution of points is used, highly irregular isotropic foams containing a wide size distribution of large and small cells will result.

It is worth noting that the tessellation of the BCC array (the tetrakaidecahedral cell model discussed above) is a reasonable approximation to the foam introduced by Lord Kelvin (Weaire and Fortes, 1994; Warren and Kraynik, 1997; Grenestedt, 1999). The cells of the Kelvin foam are uniformly shaped, fill space, and satisfy Plateau's law of foam equilibrium (three faces meet at angles of 120°, and four struts join at 109.5°). In order for this to be true, the faces and edges are slightly curved (Weaire and Fortes, 1994), unlike those of the tetrakaidecahedral cell model.

In this study, we wish to examine foams that have a roughly uniform cell size, but which are still random and isotropic. A non-periodic, evenly spaced, and isotropic arrangement and seed points is therefore necessary. Such a distribution is provided by the centre points of equi-sized hard spheres in thermal equilibrium (Torquato, 1991). If the spheres are quite closely packed the Voronoi cell size will be approximately equal to the sphere diameter d_0. The distributions were generated using a Monte-Carlo algorithm. To move a sphere we chose a set of (20) random directions and jump distances. Of the allowable jumps (i.e. those which did not overlap another sphere) we chose one at random. Each sphere was visited once during a Monte-Carlo step, and

several thousand steps were used to randomize the system. The initial conditions were defined by placing 122 spheres in a simple cubic array within a periodic cube of size $125d_0^3$. Periodic boundary conditions were employed, as well as a coarse grid array, so that only a fraction of the spheres had to be checked for overlaps prior to each jump. We checked that the resultant random packing resulted in isotropic cellular solids (see below).

A pixel in the digital model is defined as belonging to an edge if it is approximately equidistant from at least three sphere centres. The density of the model is changed by varying the thickness of the cell edges. An illustration of the open-cell model (with only 63 cells) is shown in Fig. 4(a). Since we are specifically interested in isotropic foams, we confirmed that the cell edges showed no orientational preference. This was done by measuring the probability distribution of the polar (ϕ) and azimuthal (θ) angles of each edge from a fixed direction. We found ϕ was distributed with density $\rho(\phi) = \sin\phi$ on $[0,\pi)$ and θ was uniformly distributed on $[0, 2\pi)$, which corresponds to an isotropic distribution. The maximum and average relative errors were, respectively, 9% and 5%, which we attribute to the sample sizes considered. The average strut length is $0.45d_0$, and for comparison with other models we show the entire strut-length probability distribution in Fig. 5(a).

In the low-density limit, the Young's modulus of the open-cell tessellation can be fitted by Eq. (1) to within a maximum of 5% relative error with the parameters $C = 0.930$ and $n = 2.04$ or

$$\frac{E}{E_s} = 0.930\left(\frac{\rho}{\rho_s}\right)^{2.04} \quad \text{for } 0.04 < \frac{\rho}{\rho_s} < 0.5. \tag{8}$$

The FEM data and Eq. (8) (solid line) are shown in Fig. 6. This simple scaling relation cannot reproduce the high-density behaviour ($E \to E_s$ as $\rho \to \rho_s$ unless C is fortuitously equal to one). Rather than choosing a three- or four-parameter relation to describe the full density range, we instead use the equation

$$\frac{E}{E_s} = \left(\frac{p - p_0}{1 - p_0}\right)^m \left(p = \frac{\rho}{\rho_s}\right). \tag{9}$$

which has been found useful for describing the properties at high densities. With $m = 3.12$ and $p_0 = -0.0056$, the formula describes the FEM data to within 5% for $0.04 > \rho/\rho_s < 1$. The fit is shown on Fig. 6 as a dashed line. Note that the fitting parameters p_0 and m are not the conventional percolation threshold and exponent. However, since the actual percolation threshold of the Voronoi tessellation is expected to be zero, it is interesting, but perhaps fortuitous, that the value of p_0 is quite small.

Interestingly, just like the periodic models, the bulk modulus shows a near linear decrease with density. The low-density limit of the bulk modulus can be described by Eq. (1) with $C = 0.209$ and $n = 1.22$. For the shear modulus, $C = 0.404$ and $n = 2.12$. At the lowest density ($\rho/\rho_s = 0.05$), the Poisson's ratio is relatively high ($\nu = 0.44$) and the trend indicates that $\nu \to 0.5$ as $\rho/\rho_s \to 0$.

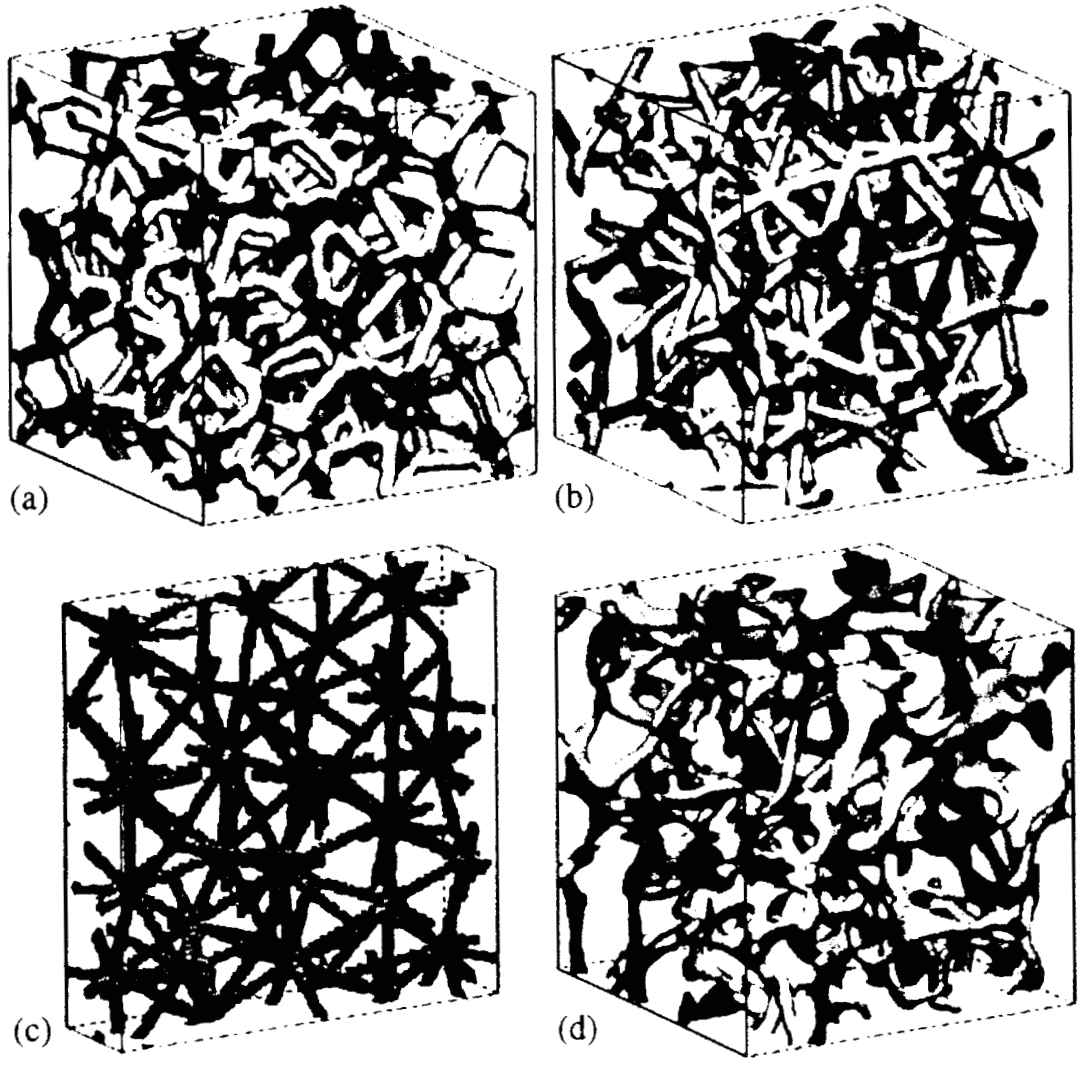

Fig. 4. Random models of open-cell solids. (a) The open-cell Voronoi tessellation with $\rho/\rho_s = 0.15$. The model shown has 6^3 cells, whereas the computations were performed on samples with 125 cells. (b) The low-coordination number ($\bar{z} = 5.5$) node-bond model with $\rho/\rho_s = 0.13$. (c) A digital model of the high-coordination number foam ($\bar{z} \approx 12$) with $\rho/\rho_s = 0.075$. (d) The open-cell Gaussian random field model with reduced density $\rho/\rho_s \approx 0.1$.

3.2. Node-bond models

As mentioned above, cellular solids are not necessarily derived from a liquid foam. For example, metallic foams may be generated by burning out particulate inclusions or infiltrating a porous matrix which is later removed by leaching. Other cellular solids, such as bone and sponge, are generated by complex organic processes (Gibson and Ashby, 1988). Since simulating the actual physics and chemistry of the development of cellular material, is beyond the scope of this paper, we instead consider three different statistical models that have features resembling those observed in real cellular solid

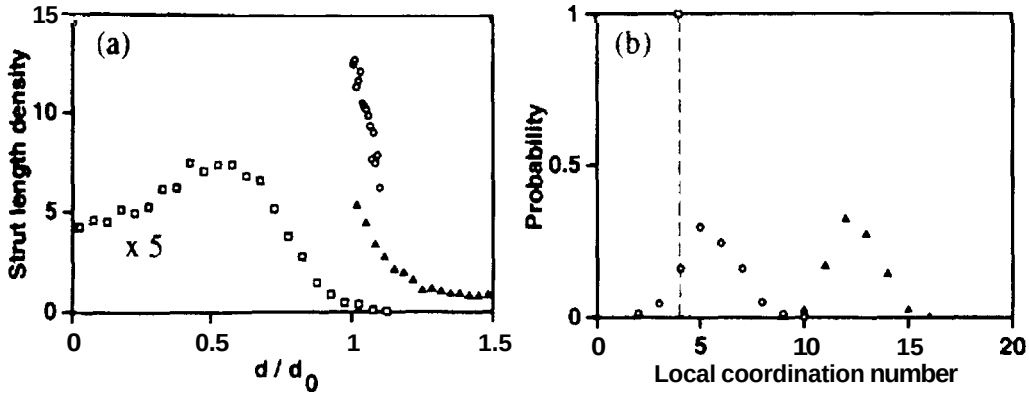

Fig. 5. (a) Strut-length probability density of three models. Data for the open-cell tessellation has been magnified by a factor of five. (b) Probability that a node has a specified coordination number. The tessellation has a local coordination number of four by definition. Models: open-cell tessellation (□); node-bond models with $\bar{z} \approx 5.5$ (○) and $\bar{z} \approx 12$ (△).

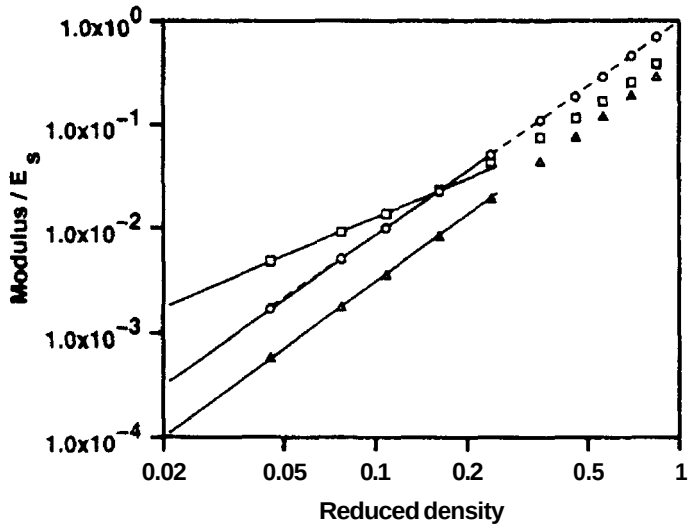

Fig 6. The Young's (○), bulk (□) and shear (△) moduli of the open-cell Voronoi tessellations. The lines dre the empirical fits to the data given in the text (see Eqs. (8) and (9))

materials. In this section, we consider node-bond models with variable coordination number (i.e. the number of bonds connected to each node) generated from random seed points.

There are several methods of generating open and closed-cell cellular models from seed points. An example is provided by the Delaunay (or Voronoi-dual) tessellation (Stoyan et al.. 1995). Starting from a Voronoi tessellation. the cell edges are now defined by a rod placed between two points in space which share a common face. Since the cells of a Voronoi tessellation have approximately 14 faces (Oger et nl., 1996). the coordination number of an open-cell Delaunay tessellation will also be around $\bar{z} \approx 14$.

It is possible to define a more general model, called in this paper a 'node-bond' model, by placing a bond between each seed (or node) and its nearest neighbours. The coordination number, average bond length, and bond-length distribution depend on the rules used for defining the nearest neighbours of a given node. For example, the coordination number z can be fixed by connecting a node to its z nearest neighbours. The coordination number can also be allowed to fluctuate if nodes are only connected when node–node distance is smaller than some specified value. If the resulting average coordination number of the foam is around 14, we expect the model to be simiiar to an open-cell Delaunay tessellation.

To be specific, we connected the centres of an equilibrium hard-sphere (diameter d_0) distribution that were closer than the distance Fd_0 ($F > 1$). We employed the same five distributions of 122 points used for the Voronoi tessellation. To generate the microstructure for the elastic computations we placed a cylinder of radius r between each pair of connected points. Hemi-spherical caps were added at each end to avoid gaps occurring between cylinders that intersect at an angle. An illustration of the node-bond model is shown in Fig. 4(b).

We first chose $F = 1.5$, which yielded a high-coordination number foam of $\bar{z} = 12.5$ with average bond length of $\bar{d}\ d_0 = 1.16$. This model is illustrated in Fig. 4(c). which is a digital model actually used in the elastic computations. To simulate a low-coordination number foam we also studied the case $F = 1.1$, which yielded $\bar{z} = 5.5$ with an average bond length of $\bar{d}\ d_0 = 1.04$ (Fig. 4(b)). Dangling branches in the model were avoided by deleting all nodes with less than two 'nearest' neighbours. The process was repeated until all nodes has two or more nearest neighbours. For $F = 1.1$. only two or three nodes were deleted from each sample. In spring lattices. this iterative removing of low-connectivity nodes has been called 'trimming' (Feng et al., 1985). For comparison with other models. the probability density of bond lengths and local coordination numbers are shown in Fig. 5.

The Young's modulus of the high-coordination number model can be described to within a 4% relative error by

$$\text{for } 0.04 < \frac{\rho}{} < 0.25 \tag{10}$$

and to within 4% for $0.1 < \rho\ \rho_s < 1$ by Eq. (9) with $p_0 = -0.198$ and $m = 2.80$. The Young's modulus of the low-coordination number model can be described to within a 5% relative error by

$$\frac{E}{E_s} - 0.535\left(\frac{\rho}{\rho_s}\right)^{1.81} \quad \text{for } 0.026 < \frac{\rho}{\rho_s} < 0.35 \tag{11}$$

and by **Eq.** (9) with $p_0 = -0.445$ and $m = 4.27$ for $0.25 < \rho\ \rho_s \leq 1$. The FEM data and Eqs. (10) and (11) are shown in Fig. 7. The behaviour of the Poisson's ratio of this model will be discussed in Section 4.

3.3. Cellular solids based on Gaussian random fields

Very different types of models can be generated using the level-cut Gaussian random field (GRF) scheme. One starts with a GRF field $y(r)$, which assigns a (spatially

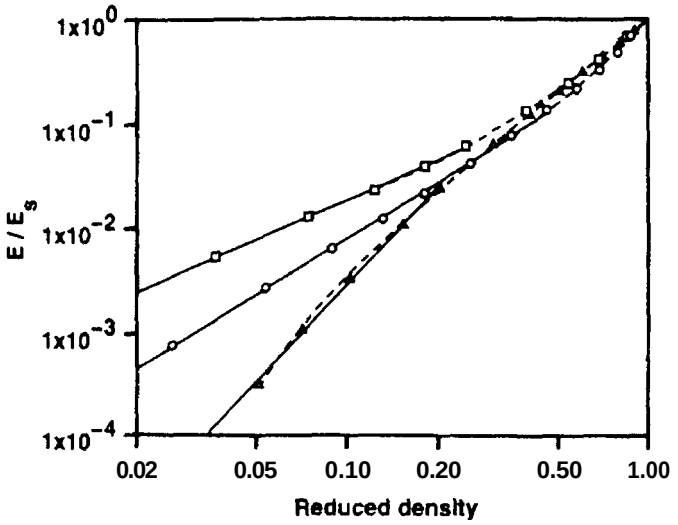

Fig. 7. The Young's modulus of the non-foam-like cellular models: high-coordination number node-bond model (□), low-coordination number node-bond (○) and Gaussian random field model (A). The lines are the empirical fits to the data given in the text.

correlated) random number to each point in space. A two-phase solid-pore model (Berk, 1987; Roberts and Knackstedt, 1996) can be defined by letting the region in space where $-\beta < y(\boldsymbol{r}) < \beta$ be solid, while the remainder $[|y(\boldsymbol{r})| \geqslant \beta]$ corresponds to the pore space. Open-cell solids can be obtained from the model by forming the intersection sets of two statistically independent level cut GRF models (Roberts. 1997). An example is shown in Fig. 4(d). Details for generating the models have been previously described (Roberts and Garboczi. 1999).

The model (Fig. 4(d)) shows a highly irregular structure. with curved 'struts' of variable thickness. The morphology is reminiscent of the nickel and copper cellular solids in Fig. 2.4 of Gibson and Ashby (1988) and the sponges shown in Fig. 2.5 (Gibson and Ashby, 1988) and Fig. 31 of Weaire and Fortes (1994). The small-angle scattering intensities of the model have also been shown to be consistent with experimental data for organic aerogels (Roberts. 1997). At low densities, the Young's modulus can be described (to within 12%) by

$$\frac{E}{E_s} = 4.20\left(\frac{\rho}{\rho_s}\right) \qquad \text{for } 0.05 < \frac{\rho}{\rho_s} < 0.20. \tag{12}$$

Eq. (9) describes the higher density data ($\rho/\rho_s > 0.2$) with $m = 2.15$ and $\rho_0 = 0.029$ to within 4% (and the low-density data to within 12%). The data and fitting formulae are shown in Fig. 7.

The data show a small. bur persistent, curvature as the density decreases below 0.2. This could be interpreted as indicting a finite percolation threshold. However, by construction. the model actually remains connected at all solid fractions. indicating that the curvature is due to resolution errors. To see that the model always percolates, note that the underlying two level-cut GRF remains connected at all finite densities. This follows from the fact that there must always be a thin surface separating the regions in

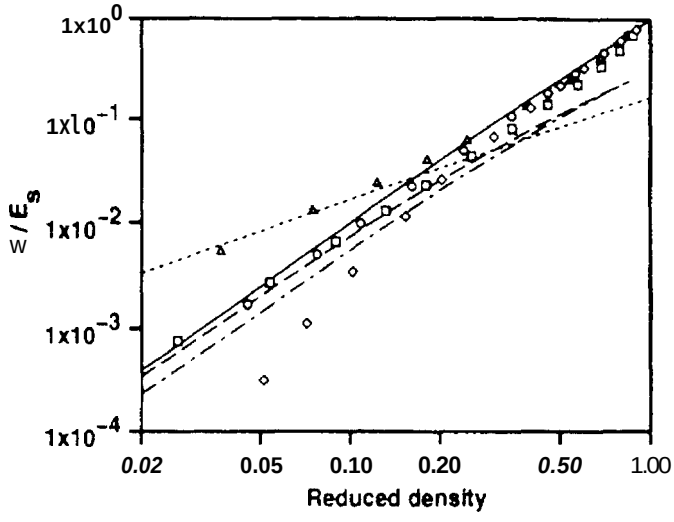

Fig. 8. Comparison of the FEM data for open-cell foams (symbols) with theory. The data shown is for the high- (△) and low- (□) coordination number node-bond models. the open-cell Voronoi tessellation (○) and the upen-cell Gaussian random field model (◇). The theories are due to Christensen (1986) (···), Gibson and Ashby (1988) (——), Warren and Kraynik (1988)(— —) and Zhu et al. (1997a) (–·–).

space where $y > 0$ and $y < 0$. The struts of the intersection model correspond to the lines where the surfaces of two independent two level-cut models intersect. Hence they will exist at all densities. and the model does not have a finite percolation threshold.

4. Comparison of FEM results with existing theory

The Young's modulus and Poisson's ratio of the open-cell foams are shown in Figs. 8 and 9 along side four relevant theories. For low densities ($0.04 < \rho/\rho_s < 0.15$), data. for the high-coordination number node-bond model (Fig. 4(c)) is reasonably well described by Christensen's results for isotropic foams with straight-through struts, indicating that longitudinal compression dominates the deformation. The power law dependence ($n = 1.3$) is higher than predicted ($n = 1$), because. being random. the model has no completely straight-throuyh struts. This does not lead to significant bending (indicated by a quadratic decay) because there are sufficient struts emanating from each node to 'lock' the relative node positions. and reduce the bending component of deformation. In contrast. data for the low-coordination number node-bond model ($0.03 < \rho/\rho_s < 0.30$) are well described by the semi-empirical result given by Gibson and Ashby (1988) ($n = 2$). This confirms the predominance of the beam-bending mechanism for deformation for this model. The Young's modulus of the open-cell Voronoi tessellation also follows the conventional quadratic decay with density, but as noted above (Fig. 6), the bulk modulus actually scales linearly with density. In contrast to Van der Burg et al. (1997), we do not find that the random tessellation is appreciably stiffer than the tetrakaidecahedral model. This may be due to the tact that our results were obtained at a minimum density around two-fold higher than that used by Van der

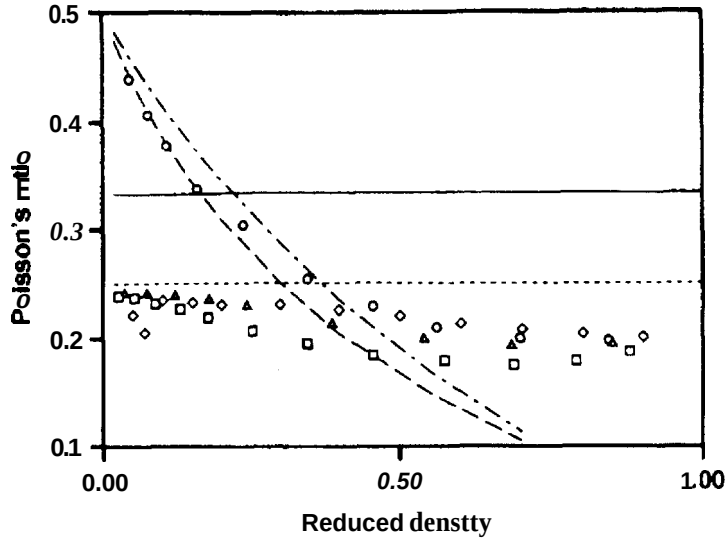

Fig. 9. Comparison of the FEM data for open-cell foams (symbols) with theory (lines). The same nomenclature as in Fig. 8 is used.

Burg et al. Moreover, the relatively small increase (2×10^{-4}) they observed would be quite hard to discern in our results.

The modulus of the open-cell GRF model is considerably lower than any of the predictions. In this case, the 'struts' of the network are themselves bent, therefore allowing greater deformation. Moreover, the struts have varying thicknesses. Since the stiffness of the struts is limited by their thinnest sections, the mass in the thickest regions contributes little to the overall stiffness. This has the effect of reducing the moduli at a given density, compared to models having struts with a uniform cross-sectional area.

Results for the Poisson's ratio of the open-cell foams shown in Fig. 9. Data for the high- and low-coordination number node-bond models and open-cell GRF model are approximately constant, showing a slight increase from the solid value of $\nu = 0.2$ (the solid value) to $\nu \approx 0.22 \sim 0.24$ at low densities. We have recently shown (Roberts and Garboczi, 2001) that the Poisson's ratio of a wide range of three-dimensional porous materials converges nearly linearly from the Poisson ratio of the solid material (ν_s) at high densities to a microstructure-dependent fixed point at low densities. Therefore, if the fixed point is close to ν_s, as it is for the three models under discussion with $\nu_s = 0.2$, ν will be nearly independent of density as observed in the data. The actual low-density limits are close to 0.25, which is predicted by numerous independent theories; see Eq. (6) for example.

In contrast, the Poisson's ratio of the open-cell Voronoi tessellation shows a sharp increase towards $\nu \approx 0.5$ with decreasing density. This is associated with the foam being much stiffer under uniform compression ($n \approx 1$ for the bulk modulus) than under shear or uniaxial compression ($n \approx 2$). A Poisson's ratio of 0.5 is the highest attainable by an isotropic material and physically means that if a cubic sample is uniaxially compressed, the decrease in volume in the direction of compression is exactly balanced by the

lateral expansion of the material in the perpendicular directions. This 'incompressible' behaviour is observed in solid rubber and in liquids, but not generally in solid foams.

The unusual density dependence of both the bulk modulus and Poisson's ratio is actually very well described by the Warren–Kraynik results [Eq. (7)] for isotropically averaged tetrahedral joints, and qualitatively similar to the results for the tetrakaidecahedral foam [Eq. (4)]. It is easy to understand the behaviour of the simple models. If the unit cell of the tetrakaidecahedral foam model is placed under uniform compression the struts are only subject to axial (not bending) deformation, and hence the bulk modulus varies linearly with density. Alternately, if equal forces are applied along each axis of the four struts of a 'perfect' tetrahedral element, the central node is not displaced and the struts are only axially compressed. This 'node-locking' will not occur under shearing or uniaxial compression, therefore allowing bending of the struts in each case.

In general, four cells touch at each node of the Voronoi tessellation (Stoyan et al., 1995), so that there are four struts associated with each node in the open-cell model. Therefore, approximating the behaviour of the model by tetrahedral elements would seem appropriate (Warren and Kraynik, 1988). However, one would expect the disorder in the random Voronoi tessellations to allow significant bending of the struts to occur under hydrostatic compression. Our results indicate that this is not the case, and it is interesting to investigate this behaviour in more detail.

To check if the effect was restricted to our choice of seed distributions, we measured the Poisson's ratio of a low-density sample where the points were uncorrelated (i.e., a Poisson distribution). The Poisson's ratio was found to only decrease by 10% (from 0.44 to 0.4) at $\rho/\rho_s = 0.05$. Given that we expect ν to increase from 0.4 at still lower densities (e.g. Fig. 9), this indicates that random Voronoi tessellations are nearly incompressible as $\rho/\rho_s \to 0$ irrespective of the underlying seed distribution. One explanation might be that the local strut arrangement is always close to a perfect tetrahedron. To check this we measured the distribution of the six inter-strut angles (five are independent). For the hard-sphere seed points used in our moduli calculations we found $\langle\chi\rangle = 110^\circ$ with standard deviation $\sigma = \sqrt{\langle\chi^2\rangle - \langle\chi\rangle^2} = 22^\circ$. For Poisson distributed seeds we found $\langle\chi\rangle = 111^\circ$ and $\sigma = 36^\circ$. These results indicate that Warren and Kraynick's assumption of tetrahedral elements works very well for quite large angular deviations (from 109°) between the struts. If the coordination number is not equal to four, one would not expect the assumption to provide a good approximation (e.g. the node-bond models). We also measured the effect of deleting struts on the Poisson's ratio of the models. For a 2% reduction in mass, the bulk modulus decreased by 22%, while the Young's modulus only decreased by 6%. A 15% reduction in mass was required to reduce the Poisson's ratio to $\nu \approx 0.33$.

5. Comparison of FEM results with experiment

To illustrate the utility of the FEM we compare the computed results to experimental data. Since real foams can have densities lower than those we are currently able to computationally study, we use the formula $E/E_s = C(\rho/\rho_s)^n$ to extrapolate the results. This is justified by the fact that the low-density FECI data appear to fall on a straight

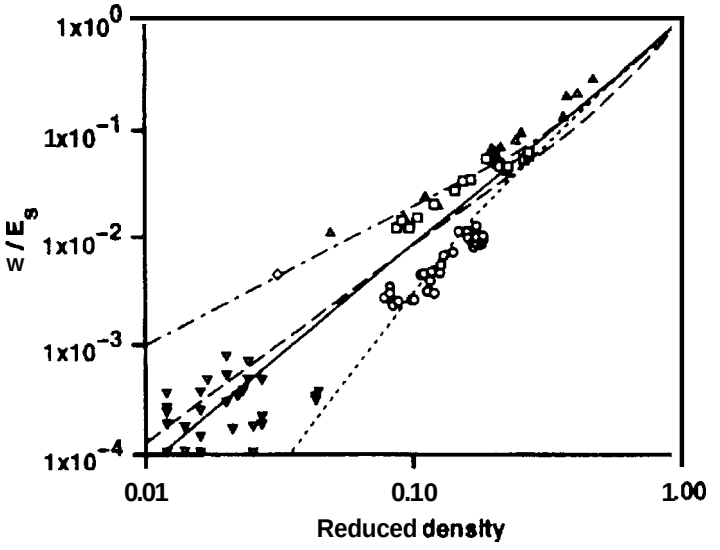

Fig. 10. Young's modulus of open-cell foams. The data is for alumina (Hagiwara and Green, 1987) (○, $E_s = 380$ GPa, $\rho_s = 3970$ kg/cm^3), rubber latex obtained by Lederman (1971) (□) and Gent and Thomas (1959) (△), open-cell foams (Gibson and Ashby, 1982) (▽), and reticulated vitreous carbon (Christensen, 1986) (◇, $E_s = 6.9$ GPa). The lines corresponds to the four open-cell FEM theories derived in this paper; high (– · –) and low (– – –) coordination number foams, open-cell Voronoi tessellation (——) and the open-cell Gaussian random field model (· · ·).

line when plotted against log–log axes. Accurate comparison of theoretical and experimental results is hindered by the imprecision involved in estimating the properties of the solid skeleton, E_s and ρ_s. We report E_s and ρ_s when they have been given. but some data sets are reported only in terms of E/E_s and ρ/ρ_s. Some of the data sets we have taken from the literature have been previously summarised (Gibson and Ashby, 1988; Green, 1985).

Data for open-cell foams are compared with the open-cell FEM derived theories in Fig. 10. The data for rubber latex foam lies above the line $E/E_s = (\rho/\rho_s)^2$ and agree reasonably well with the FEM result for high-coordination number node-bond models. If the estimated value of E_s is correct. this suggests that the coordination number of the foam is quite high. The single data point (◇) obtained for a carbon foam (Christensen, 1986) falls on the same line. A micrograph in the reference indicates that the struts were tetrahedrally coordinated. unlike the model. Note that the normalisation constant $E_s = 6.9$ GPa used by Christensen seems low compared to the value $K_s = 24$ GPa ($E_s = K_s$ if $\nu = \frac{1}{3}$) adopted for carbonised aerogels (Pekala et al., 1990). Indeed. if $E_s = 24$ GPa is assumed, the data points falls close to the line $E/E_s = (\rho/\rho_s)^2$.

The data for porous alumina agree reasonably well with the predictions of the open-cell GRF model. However, micrographs of the structure indicate a structure closer to that of the open-cell Voronoi tessellation (with occasional closed faces). so the agreement seems fortuitous. Data for the open-cell materials considered by Gibson and Ashby (1982) is seen to agree well with the FEM results for the low-coordination number node-bond model and open-cell Voronoi tessellation.

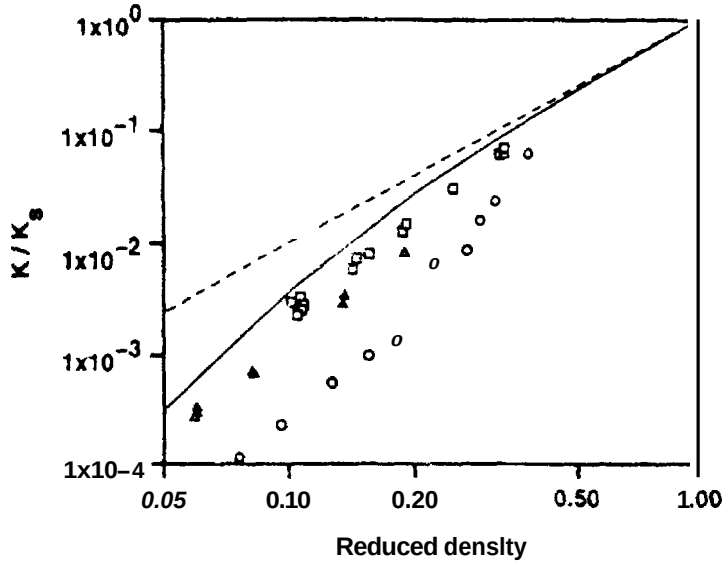

Fig. 11. Bulk modulus of open-cell aerogel foams. The data is for carbonized (□, $K_s = 24$ GPa, $\rho_s = 1500$ kg cm^3) and uncarbonized organic aerogels (△, $K_s = 3.5$ GPa, $\rho_s = 1300$ kg cm^3) (Pekala et al., 1990). The circles corresponds to data from Gross et al. (1997) for an uncarbonized organic aerogel prepared under different conditions. The lines correspond to the open-cell Gaussian random field (——) and the conventional theory $K/K_s = (\rho/\rho_s)^2$ (– – –).

In a prior paper (Roberts, 1997), it was suggested that open-cell GRF's provide useful models of organic aerogels. It was shown that the models could reproduce the scattering intensities and predict the contribution of the solid network to the overall thermal conductivity of these low-density materials. These prior results provide evidence that the model is reasonable, but it is also important to compare the elastic properties with experimental data. Data for the bulk modulus of open-cell organic aerogels is compared with the FEM results in Fig. 11. We have assumed that $K/K_s = E/E_s$, which corresponds to the assumption that Poisson's ratio is constant with density [$\nu(\rho/\rho_s) = \nu_s$], which we have shown to be approximately true at low density. The FEM results over-estimate the data for 'polymeric' aerogels (Pekala et al., 1990) by factors of 2.4 and 1.5 for samples before and after carbonisation, respectively. However, the decay of modulus with density is reasonable, indicating that the basic structure of the model is correct, but that there is more elastically inefficient mass in the real materials (such as dangling ends, or struts of non-uniform width). The microstructure (and elastic properties) of aerogels are highly variable, and the data shown is for the stiffest structures. For example, data is also shown for a 'collidal' aerogel in the figure. The struts of colloidal aerogels tend to be granular, with the narrow inter-particle necks decreasing the overall stiffness. Note that the random-field model can be modified to mimic this type of structure by shifting the position of the level cuts (Roberts, 1997).

In Fig. 12, we compare measurements of Poisson's ratio for various foams with the FEM results. In general, it is difficult to measure ν, and there is significant scatter in the data (Gibson and Ashby, 1988). For low densities, ν becomes practically independent of ν_s (Roberts and Garboczi, 2001). For example, the open-cell CRF model

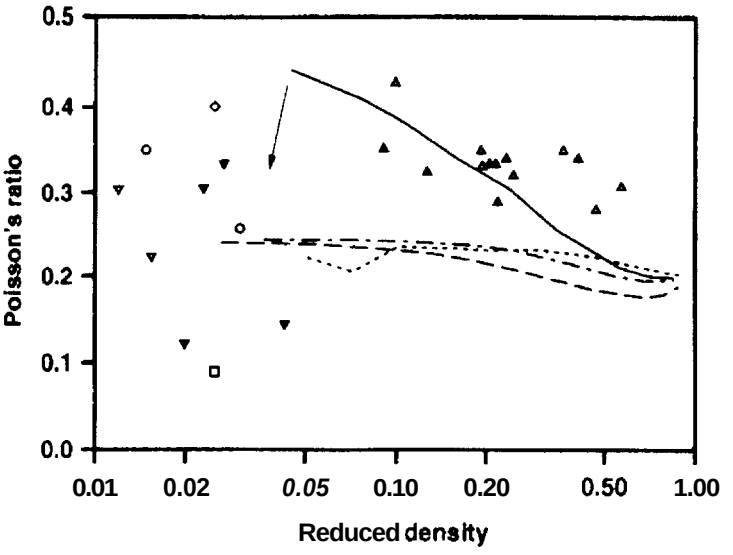

Fig. 12. Poisson's ratio of open-cell foams. The data is for various forms of polyurethane (Gibson and Ashby, 1982) (▽), (Zhu et al., 1997b) (□), (El-Rata1 and Mallick, 1996) (○), rubber latex (Gent and Thomas, 1959) (△), and an open-cell polymer **foam** (Lakes, 1987). The lines corresponds to the four open-cell FEM theories derived in this paper: high- (– · –) and low- (– – –) coordination number **foams. the** open-cell Gaussian random field model (· · ·) and the open-cell Voronoi tessellation (——). The arrow represents **the** effect of deleting 15% of the struts from the tessellation.

has $\nu = 0.23 \pm 0.03$ for $\rho/\rho_s < 0.2$ (the variation decreasing linearly with density). It is therefore meaningful to compare our computations and experimental data at low density irrespective of ν_s. The predictions of the node-bond models and open-cell GRF model ($\nu \approx 0.25$) lie amongst the scattered data, but the open-cell tessellation has a lower compressibility (i.e. ν is closer to 0.5) than any foam for which we have data. Since Voronoi tessellations are most commonly used to model foams, it is interesting to note that the model appears to over estimate experimental Poisson's ratios. **It** may be that real foams contain broken struts, due to imperfections in the solidification process. We have shown that ν decreases to 0.33 if 15% of the struts are removed. Alternatively, foams may have sufficiently curved struts to allow bending under uniform compression. We consider this possibility below.

The struts of true surface-energy minimising foams, such as those shown in Figs. 27 and 29 of Weaire and Fortes (1994), show very slight curvature (the maximum deviation δ appears to be less than 5% of the bond length l). The curvature will only be significant (i.e. allow bending) if the strut diameter d is around the same size as the axial deviation ($\delta \times l$). For the tetrakaidecahedral model, the struts have length $l = T/2\sqrt{2}$, and the reduced density is $\rho/\rho_s = 3\pi d^2/\sqrt{2}T^2$, where T is the size of the unit cell shown in Fig. 1(d). Setting $d = \delta \times l$ and $\delta = 0.05$ we find that curvature will only significantly alter the axial stiffness of the strut if $\rho/\rho_s < 3\pi\delta^2/8\sqrt{2} = 0.0021$. Since most cellular solids have $\rho/\rho_s > 0.01$, the proposed strut curvature should not be significant. Moreover, even if the struts are curved, both the Young's and bulk modulus will decrease (possibly leaving Poisson's ratio $\nu = 1/2 - E/6K$ unchanged). Indeed, Grenestedt (1998) has shown that the ratio E/K is constant for a simple open-cell

model with curved beams. Hence, it seems unlikely that the natural strut curvature of foams would significantly reduce Poisson's ratio.

6. Discussion and conclusion

We have used the finite element method to estimate the Young's modulus of four realistic random models of isotropic cellular solids. The open-cell Voronoi tessellations have a microstructure similar to that observed in foams. The node-bond and level-cut Gaussian models were considered representative to cellular solids generated by other (non-foaming) processes. At low densities, the results could be described by the scaling relation $E/E_s = C(\rho/\rho_s)^n$, where C and n are given in the text. At moderate to high densities, the results could be described by Eq. (9) using the parameters reported in the text. The fitting relations we have derived can be used to predict the properties of cellular materials that have a microstructure similar to one of the models, and can be useful for interpreting experimental data.

We have compared the results to a number of theories based on different simplifying assumptions about microstructure. The most widely used formula for the Young's modulus of open-cell materials is $E/E_s = (\rho/\rho_s)^2$, with a Poisson's ratio of $\nu = 0.33$ (independent of density and solid Poisson's ratio ν_s). While this result is broadly applicable, we have shown that the properties of open-cell materials are more complex. The highly coordinated ($z = 12.5$) node-bond model has an exponent of $n = 1.3$ due to spatial 'locking' of the nodes, so that the major mechanism of deformation is axial tension (or compression) rather than bending. The open-cell random field model, which is not based on an underlying polyhedral structure, had an exponent of $n = 3.0$. This was attributed to enhanced deformation in the struts, which are curved and have non-uniform thickness. For three of the four open-cell models, the Poisson's ratio converged to $\nu = 0.25$ at low densities, in agreement with several independent theories. The fact that the solid Poisson's ratio was taken to be 0.2 meant that the overall Poisson's ratio was nearly independent of density. If the solid Poisson's ratio was much different, the overall Poisson's ratio would be a much stronger function of density, because of its convergence or 'flow diagram' behaviour (Roberts and Garboczi, 2001).

One of the most surprising results was that isotropic open-cell Voronoi tessellations were nearly incompressible (Poisson's ratio $\nu \approx 0.5$) at low densities. In hindsight, the result might be anticipated from two-dimensional studies of random two-dimensional tessellations for which $\nu_{2D} \approx 0.94$ (Silva et al., 1997). The near incompressibility of the tessellations is related to the fact that the structure is much stiffer under uniform compression than axial (or shear) deformation ($K \propto \rho$ while $E, G \propto \rho^2$). At low densities, the properties of the model foam are actually very well predicted by Warren and Kraynik's theoretical result for an isotropically oriented tetrahedral joint. This provides an explanation of the unusual behaviour. In a perfect tetrahedral joint under uniform compression, the forces are balanced so that the central node is locked in position. Therefore, the deformation is only along the strut directions (i.e. $h \propto \rho$). Even though the struts in the random model are not perfectly tetrahedral, we have shown that the same node locking occurs on average. Our results indicate that broken, rather than bent,

struts provide a more likely explanation of why such high values of the Poisson's ratio are not commonly observed.

In this study, we have shown that it is absolutely necessary to consider large-scale (multi-cellular) models of random cellular solids in order to obtain realistic elastic properties. Our results are consistent with experimental data, and show a more complex density dependence than predicted by conventional theories based on periodic cell models. Our results focus on the global (e.g. connectivity and geometrical cell arrangement), rather than local characteristics (e.g. strut cross-sectional shape or curvature) of cellular materials, for the following reasons. First, it is difficult to simultaneously model the local and global variables with finite computational power, and second, study of single-cell models probably provides a more fruitful route to understanding the influence of local cell character on the overall properties. We believe that the results of both approaches may be beneficially combined.

Acknowledgements

A.R. thanks the Fulbright Foundation and Australian Research Council for financial support. We also thank the Partnership for High-Performance Concrete program of the National Institute of Standards and Technology for partial support of this work.

References

Berk, N.F., 1987. Scattering properties of a model bicontinuous structure with a well defined length scale. Phys. **Rev.** Lett. 58, 2718–2721.

Chen, C., Lu, T.J., Fleck, N.A., 1999. Effect of imperfections on the yielding of two-dimensional foams. J. Mech. **Phys.** Solids 47, 2235–2272.

Christensen, R.M., 1986. Mechanics of low density materials. J. Mech. Phys. Solids 34 (6), 563–578.

Christensen, R.M., 2000. Mechanics of cellular and other low density materials. Int. J. Solids Struct. 37, 93–104.

El-Ratal, W.H., Mallick, P.K., 1996. Elastic response of **flexible** polyurethane foams in uniaxial tension. J. Eng. Mater. Technol. 118, 157–161.

Feng, S., Thorpe, **M.F.,** Garboczi, E.J., 1985. Effective medium theory **of** percolation on central-force elastic networks. Phys. Rev. B 31, 276–283.

Garboczi, E.J., 1998. NIST Internal Report 6269, available at http: ciks.cbt.nist.gov monograph (Chapter 2).

Garboczi, E.J., Day, A.R., 1995. An algorithm for computing the effective linear elastic properties of heterogeneous materials: three-dimensional results for composites with equal phase Poisson ratios. J. Mech. Phys. **Solids** 43, 1349–1362.

Gent, A.N., Thomas, A.G., 1959. The deformation of foamed elastic materials. J. Appl. Polym. Sci. 1, 107.

Gibson, L.J., Ashby, M.F., 1982. The mechanics **of** three-dimensional cellular materials. Proc. R. Soc. Lond. Ser. A 382, 43–59.

Gibson, L.J., Ashby, M.F., 1988. Cellular Solids: structure and properties. Pergamon Press, Oxford.

Green, D.J., 1985. Fabrication and properties of lightweight ceramics produced by sintering of **hollow** spheres. J. Am. Ceram. Soc. 68 (7), 403.

Grenestedt, J.L., 1998. Influence of wavy imperfections in cell walls on elastic stiffness of cellular solids. J. Mech. Phys. Solids 46 (1), 29–50.

Grenestedt, J.L., 1999. Effective **elastic** behavior of some models **for** 'perfect' cellular solids. Int. J. Solids Struct. 36, 1471–1501.

Gross, J., Scherer, G.W., Alviso, C.T., Pekala, R.W., 1997. Elastic properties of crosslinked resorcinol-formaldehyde gels and aerogles J. Non-Cryst. Solids 211, 132–142.

Hagiwara, H., Green, D.J., 1987. Elastic behavior or open-cell alumina J. Am. Ceram. Soc. 70 (11), 811–815.

Ko, W.L., 1965. Deformations of foamed elastomers J. Cell. Plast. 1, 45–50.

Lakes, R., 1987. Foam structures with a negative Poisson's ratio. Science 235, 1038–1040.

Landau, L.D., Lifshitz, E.M., 1959. Theory of Elasticity, Pergamon, London.

Lederman, J.M., 1971. The prediction of the tensile properties of flexible foams J. Appl. Polymer Sci. 15, 693–703.

Nieh, T.G., Kinney, J.H., Wadsworth, J., Ladd, A.J.C., 1998. Morphology and elastic properties of aluminum foams produced by a casting technique. Scr. Mater. 38 (10), 1487–1494.

Oger, L., Gervois, A., Troadec, J.P., Rivier, N., 1996. Voronoi tessellation of packings of spheres topological correlation and statistics. Philos. Mag. B 74, 177–197.

Pekala, R.W., Alviso, C.T., LeMay, J.D., 1990. Organic aerogels microstructural dependence of mechanical properties in compression. J. Non-Cryst. Solids 125, 67–75.

Poutet, J., Manzoni, D., Hage-chehade, F., Jacquin, C.G., Bouteca, M.J., Thovert, J.F., Adler, P.M., 1996. The effective mechanical properties of random porous media. J. Mech. Phys. Solids 44, 1587–1620.

Roberts, A.P., 1997. Morphology and thermal conductivity of model organic aerogels. Phys. Rev. E 55, 1286–1289.

Roberts, A.P., Garboczi, E.J., 1999. Elastic properties of a tungsten-silver composite by reconstruction and computation. J. Mech. Phys. Solids 47 (10), 2029–2055.

Roberts, A.P., Garboczi, E.J., 2001. Computation of the linear elastic properties of random porous materials with a wide variety of microstructure, in preparation.

Roberts, A.P., Knackstedt, M.A., 1996. Structure-property correlations in model composite materials. Phys. Rev. E 54, 2313–2328.

Silva, M.J., Hayes, W.C., Gibson, L.J., 1997. The effects of non-periodic microstructure and defects on the elastic properties of two-dimensional cellular solids. Int. J. Mech. Sci. 37 (11), 1161–1177.

Stoyan, D., Kendall, W.S., Mecke, J., 1995. Stochastic Geometry and its Applications, 2nd Edition. Wiley, Chichester.

Torquato, S., 1991. Random heterogeneous media: microstructure and improved bounds on effective properties. Appl. Mech. Rev. 44, 37–76.

Van der Burg, M.W.D., Shulmeister, V., Van der Geissen, E., Marissen, R., 1997. On the linear elastic properties of regular and random open-cell foams models. J. Cell. Plast. 33, 31–54.

Warren, W.E., Kraynik, A.M., 1988. The linear elastic propenies of open-cell foam J. Appl. Mech. 55, 341–346.

Warren, W.E., Kraynik, A.M., 1997. Linear elastic behavior of a low density Kelvin foam with open cells J. Appl. Mech. 64, 787–794.

Warren, W.E., Neilsen, Z.K., Kraynik, A.M., 1997. Torsional rigidity of a Plateau border Mech. Res. Comm. 24, 667–672.

Weaire, D., Fortes, M.A., 1994. Stress and strain in liquid and solid foams. Adv. Phys. 43 (6), 685–738.

Zhu, H.X., Knott, J.F., Mills, N.J., 1997a. Analysis of the elastic properties of open-cell foams with tetrakaidecahedral cells J. Mech. Phys. Solids 45, 319–343.

Zhu, H.X., Mills, N.J., Knott, J.F., 1997b. Analysis of the high strain compression of open-cell foams. J. Mech. Phys. Solids 45, 1875–1904.